On the Eutectic Solidification of Spheroidal Graphite Iron– An Experimental and Mathematical Modeling…

Chapter · April 2001

CITATIONS
16

READS
460

4 authors:

Roxana Ruxanda
Emerson
24 PUBLICATIONS **297** CITATIONS
SEE PROFILE

Lazaro Beltran-Sanchez
Intel
7 PUBLICATIONS **242** CITATIONS
SEE PROFILE

J. Massone
Universidad Nacional de Mar del Plata
35 PUBLICATIONS **152** CITATIONS
SEE PROFILE

Doru M. Stefanescu
The Ohio State University
364 PUBLICATIONS **4,062** CITATIONS
SEE PROFILE

Trans. AFS, **109** (2001) 1037-1048

On the Eutectic Solidification of Spheroidal Graphite Iron

– An Experimental and Mathematical Modeling Approach –

Roxana Ruxanda, Lazaro Beltran-Sanchez, Juan Massone, and Doru M. Stefanescu
The University of Alabama, Tuscaloosa, Al.

ABSTRACT

The sequence of solidification of spheroidal graphite iron is discussed based on existing theories. Then, using the results of SEM investigation of micro-shrinkage regions in thin plates ductile iron, and of metallographic investigation using color-etching metallography, the authors provide a detailed description of the eutectic grain in ductile iron. It was found that the eutectic structure of ductile iron includes primary austenite dendrites as well as eutectic dendrites containing several nodules. A computational solidification model that describes microstructure evolution of the multi-nodule eutectic grains in ductile iron was also proposed. The model generates calculated microstructures that correctly depict the experimental microstructure obtained through SEM and color-etching metallography.

INTRODUCTION

The theories regarding solidification for spheroidal graphite (SG) iron have been reviewed repeatedly over the last years (Stefanescu, 1988, Van de Velde, 1997). It is apparent that researchers agree that both graphite and austenite nucleation occurs in the liquid. However, there are a variety of opinions regarding the nucleation sequence: graphite spheroids nucleate first, followed by austenite (Loper, 1962), both nucleate at the same time (Stefanescu, 1990) or austenite nucleates first (Fredriksson, 1988). Further disagreement exists regarding the exact location of nucleation of the phases: it may be spatially random or on preferred sites (Patterson, 1952), independently (Stefanescu, 1990, Boeri, 1989), or one because of the other (Stefanescu, 1992, Rickert, 1985).

It is agreed that the growth of the two phases is strongly related. Older theories were postulating the presence of a single graphite nodule encapsulated in an austenite shell (*e.g.*, Lux, 1974), whereas the newer theories accept the fact that the austenite grain contains several graphite nodules (Stefanescu, 1990). Graphite location with respect to the austenite dendrite, the time of the development of the austenite envelope, and the controlling growth mechanism for graphite, are still to be clarified. From the currently available information the following sequence of solidification of SG iron can be postulated (Stefanescu, 1992):

- Both austenite grains and graphite nodules nucleate in the liquid.
- Growth of the nodules in contact with the liquid appears to be limited.
- Most of the nodules then attach to dendrites, growing at the dendrite-liquid interface.
- Finally, the nodules are incorporated in the austenite dendrite and further growth is possible by diffusion through the austenite shell.

Austenite and graphite nodules grow as a divorced eutectic, without coupled growth of the two phases at the solid-liquid interface. After the end of solidification, during the solid-state transformation the austenite phase changes into ferrite and secondary cementite. The solidification structure of SG iron cannot be easily revealed because these new phases obscure the primary structure.

Most solidification models for SG iron calculate the growth of a spherical SG-austenite aggregate (*e.g.*, Chang 1992, Charbon 1997).However, there is now enough evidence showing that the eutectic grain contains in fact more than a single nodule (Van de Velde, 1997, Rivera, 1997). The aggregation of nodules changes the geometry of the eutectic grain, from that of a sphere to a more complicated one. Therefore, a realistic solidification model of ductile iron should include not only the physics described in the preceding paragraphs, but also the non-spherical geometry of the eutectic grain containing more than a single nodule.

Prediction of the microstructure of SG iron at the microscopic scale has been approached following two major models: deterministic, and more recently, stochastic models. Deterministic models calculate average values for the important variables inside a given control volume. Among the advantages of these models, we find well-defined results, and the

smoothing effect of considering average values over a volume. Additionally, these models are relatively easy to implement in a computational program, and deliver a fast solution. Their major limitation is the lack of accuracy in describing the physics and the geometry of the microstructure. These models usually require simplifications to find the solution of the equations describing the problem, such as a specified shape for the grains (Fras, 1995, Chang, 1992, Wang, 1996).

In the particular case of the solidification of SG iron, the geometry of the eutectic grain is assumed spherical, with a single nodule at the center (Fras, 1995, Chang, 1992, Fras, 1999). While this representation can describe the growth mechanism for the divorced eutectic in SG iron, it cannot describe precisely the topology and interactions of the eutectic grains.

Stochastic models are based on Monte Carlo simulation or on Cellular Automaton rules (CA). Both use an array of cubic (3-D) or square (2-D) cells, describing the geometry of the casting. The cells are assigned an index describing their liquid, solid or transition state. CA models use deterministic laws in combination with stochastic. Grain growth (Gandin, 1998) or dendritic growth (Stefanescu, 1998) can be simulated, depending on the length scale of the model. These models have the capability of realistic representation of the solidification process, transforming the computer into a dynamic microscope.

The goal of this research was to clarify certain details of the mechanism of solidification of the SG iron eutectic and to develop a microscopic stochastic computer model that will output a realistic representation of the microstructure evolution during solidification. The main feature of the model is its ability to describe the growth of non-spherical eutectic grains containing more than one nodule.

EXPERIMENTAL WORK

Two approaches were used to obtain a clear understanding of the morphology of the austenite-graphite eutectic grain in SG iron. First, an SEM investigation was conducted on fractured surfaces in regions with micro-shrinkage, which reveal the phase morphology at the end of solidification. Then, the color etching technique was used on metallographic samples to visualize and quantify the microstructure of the eutectic grains.

SEM INVESTIGATION OF EUTECTIC MORPHOLOGY AT THE END OF SOLIDIFICATION

Information about the eutectic solidification of SG iron can be obtained by examining the 3-dimensional structure of the austenite-graphite grain. Different methods can be used to visualize the spatial dendrite shape, e.g., interrupted solidification (Van de Velde, 1997, Tian, 1992), heating/etching techniques (Schmidt, 1985), real-time X-ray topography (Kobayashi, 1987). In this paper, a SEM investigation was conducted on fractured surfaces of ductile iron tensile specimens where micro-shrinkage was found. Micro-shrinkage is a region where a mass deficit develops because of solidification contraction. It produces the effect of interrupted solidification. This provides a glimpse at the solid/liquid interface before the end of solidification.

To this purpose, a number of cast iron plates 25mm wide, 100mm long, and ranging in thickness from 2.3 to 7mm, having the chemical compositions given in Table 1, were fractured under tensile stress. Note the high carbon equivalent used to avoid carbides in the thin sections. A typical fracture exhibiting micro-shrinkage is presented in Fig. 1, at two different magnifications.

A close look within the micro-shrinkage reveals two types of dendrites exhibiting non-similar morphologies. Based on their particular shape, they were called *primary austenite dendrites* and *eutectic SG grains.* The morphology of the primary austenite dendrites is a typical one for dendrites in metallic alloys. They exhibit clear primary and secondary arms, as shown in Fig. 2. The arms have the classic parabolic tip characteristic for single-phase dendrites.

The eutectic SG grains, Fig. 3, have a significantly different morphology than the primary dendrites. They are thick and rounded, suggesting a cauliflower shape. While displaying branching, there is no clear distinction between primary and secondary arms. It appears that the SG grains are made of several graphite nodules surrounded by quasi-spherical austenite envelopes. This multi-nodular morphology of the SG eutectic grain is shown in more detail in Fig. 4.

COLOR ETCHING METALLOGRAPHY

The next goal of this research was to generate some quantitative data on the number of nodules within a eutectic grain. Because of the eutectoid transformation, the austenite grains resulting from the eutectic solidification of SG iron are no longer identifiable on the room temperature microstructure. However, color etching metallographic techniques can be used to trace the primary segregation, which is not affected by solid-state transformation.

The principle of color metallography is to produce an oxide layer of variable thickness on the surface of the sample that will decompose the light beam, thus producing interference colors. The oxide layer is obtained by chemical reaction between the metallographic reagent and the sample. Its thickness depends on the local chemical composition. Based on colors, several features can be identified on the microstructure: phases, compounds, grain boundaries, etc.

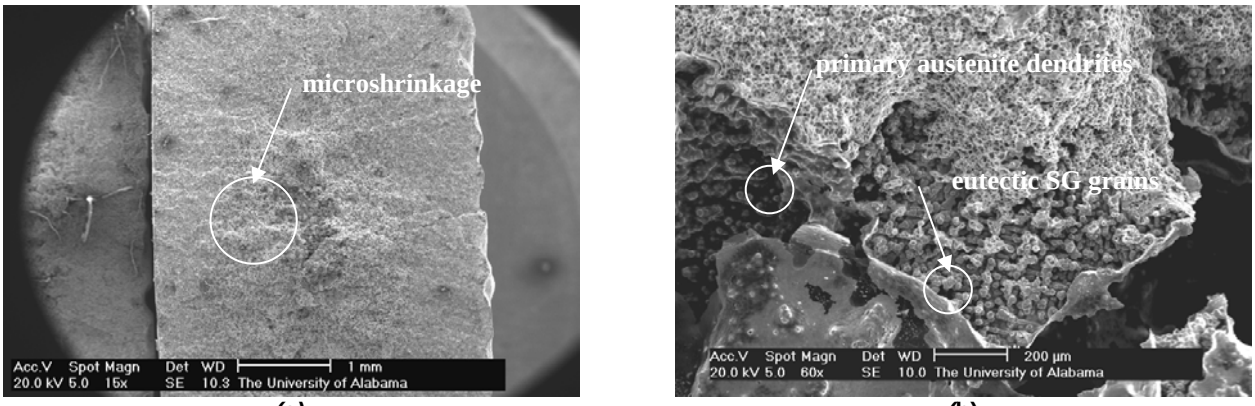

(a) ***(b)***

Fig. 1. Fractured surfaces of a ductile iron plate: (a) micro-shrinkage in tensile fractured SG iron and (b) micro-shrinkage showing primary austenite dendrites and eutectic SG grain.

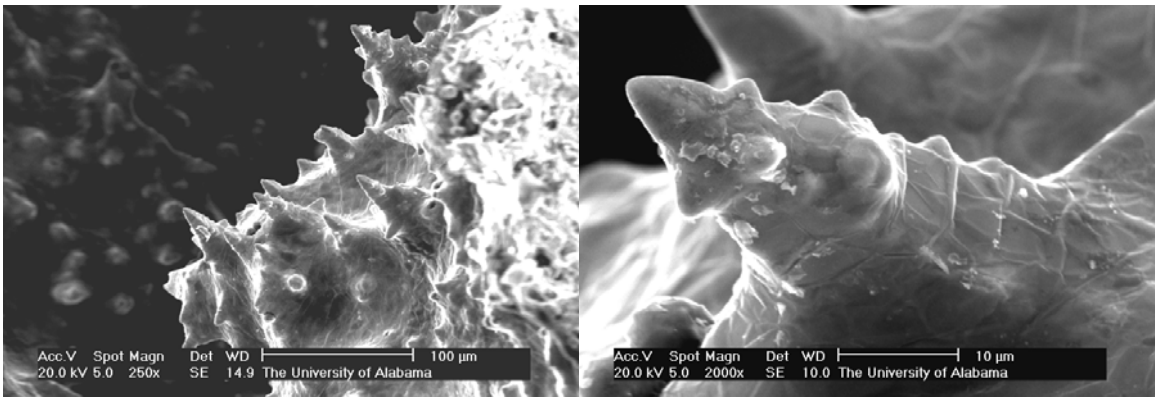

(a) ***(b)***

Fig. 2. Primary austenite dendrites. Detail from Fig. 1(b).

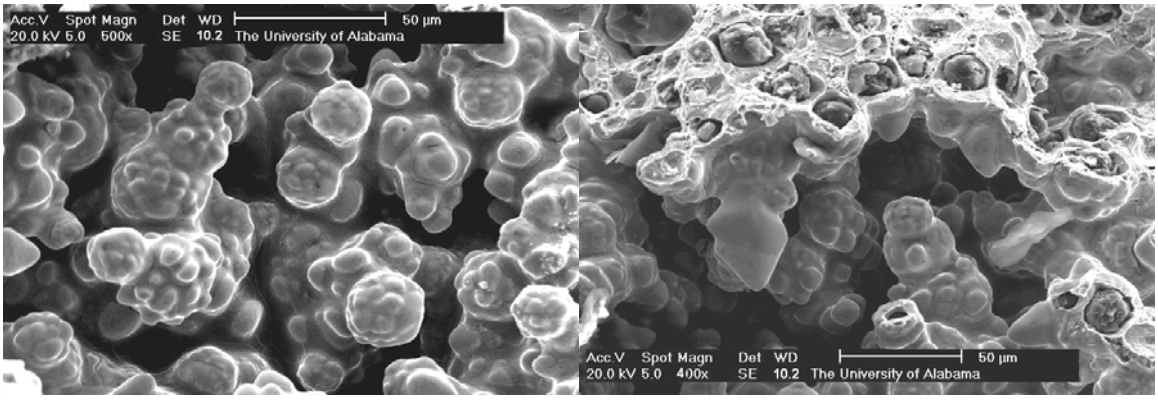

(a) ***(b)***

Fig. 3. Eutectic SG grains. Detail from Fig. 1(b).

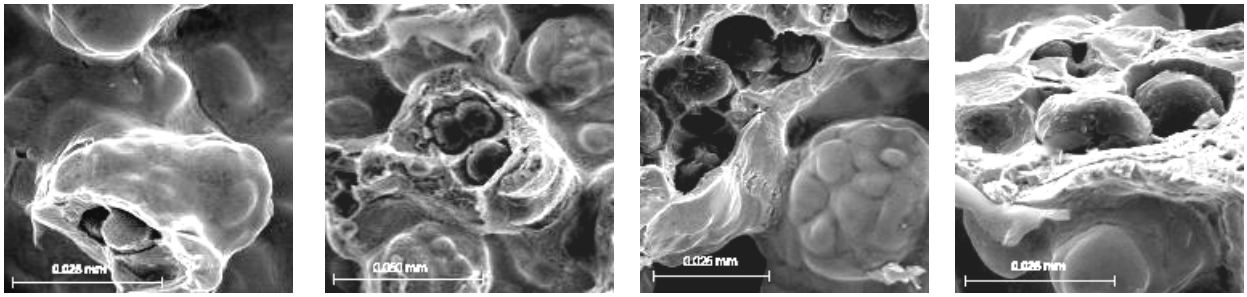

(a) ***(b)*** ***(c)*** ***(d)***

Fig. 4. Multi-nodular eutectic SG grains (SEM pictures).

Table 1. Chemical Composition of the Tensile Test Plates

C [%]	Si [%]	Mn [%]	P [%]	S [%]	Mg [%]
3.27	4.38	0.22	0.015	0.012	0.043

Table 2. Experimental Results from Color Etching

Thickness [mm]	Modulus	Nodules/grain	Nodules/mm^2	Grains/mm^2
2.3	1.15	2.98	1843	618
4.2	2.1	3.68	1256	340

Rivera (Rivera, 1997) reported that a color etching technique based on Motz reagent (Motz, 1988) is best suited to reveal the solidification structure of SG iron, as this reagent is particularly sensitive to silicon segregation. The silicon content is decreasing from the center of the grain towards the boundary, where the last to freeze (LTF) liquid regions have the lowest content. Hence, the LTF regions and some of the grain boundaries can be recognized, since from the center of the grain to the LTF region the sequence of colors is as follows: yellow, green, red, orange, bright yellow. To properly map the grains it is necessary first to identify each LTF zone, then to outline the original grain boundaries. Better results are reported if the primary segregation is analyzed in a single-phase matrix (*e.g.*, ferrite).

The method proposed by Rivera was applied on metallographic samples taken from the center of three different tensile test plates. The samples were immersed and held for several minutes at the boiling temperature (120^{o}C) in Motz reagent (10gr NaOH, 40gr KOH, 10gr picric acid, 50 ml distilled water), until the colors appeared on the polished surface. The black-and-white conversion of the color microphotograph of the 7 mm thickness sample is shown in Fig. 5 (*a*), where the silicon segregation at the LTF is clearly visible as white regions (bright yellow on the color picture). The manual adjustments made to visualize the grains are presented in Fig. 5 (*b*). It is obvious that each austenite grain contains several graphite nodules.

The number of nodules per grain was counted in all plates. The mean value was quoted as a 95% confidence interval. The number of grains per unit area was calculated as the ratio between the average number of nodules per unit area and the mean value of nodules per grain. A detailed description of the quantification technique can be found in (Rivera, 1997).
The results are presented in Table 2, where the thickness is also expressed in terms of casting modulus (volume/cooling area of casting). This was done so that our results on plates could be compared with results of other researchers on cylindrical bars.

In Fig. 6 the grain count, nodule count, and number of nodules per grain are plotted against casting modulus using the present data and previously published data (Rivera, 1997). In this manner, a larger range of moduli could be used. The abrupt change in the slope of the curves at a modulus of about 4 mm occurs because the two data sets are coming from cast irons having two different compostions. It is seen that the grain count decreases faster with modulus than the nodule count, which shows the refinement of the structure with decreasing section size.

A possible limitation of the color etching technique comes from the difficulty to distinguish between interdendritic and eutectic grain boundary segregation of silicon. Thus, the number of grains per unit area may be slightly smaller than the values shown in Table 2. Yet, the number of nodules per grain may be accepted as being an upper limit and used as such to allow the comparison with values provided by solidification modeling techniques.

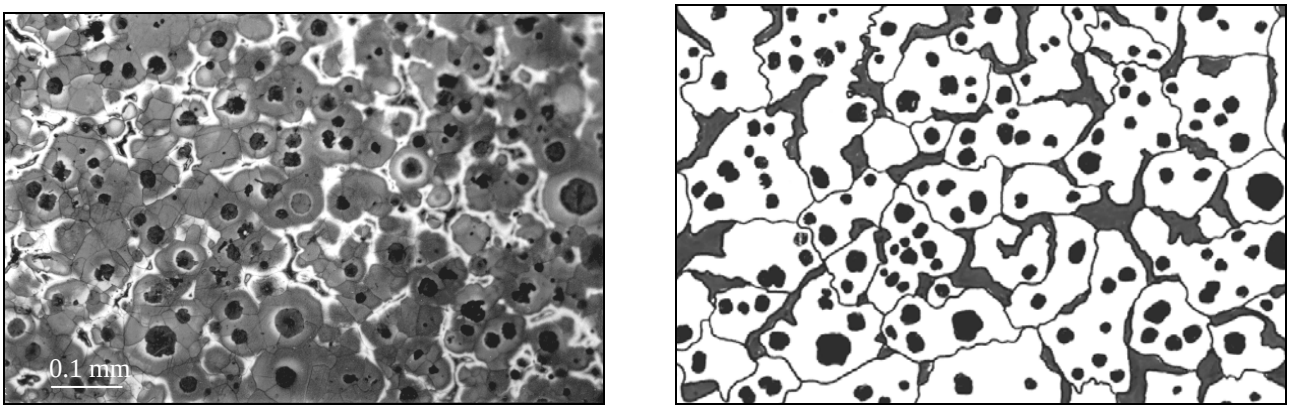

Fig. 5. Microstructure of the plates after color etching: (a) the microstructure of the 7 mm thickness sample after color etching and (b) grain and segregation delineation.

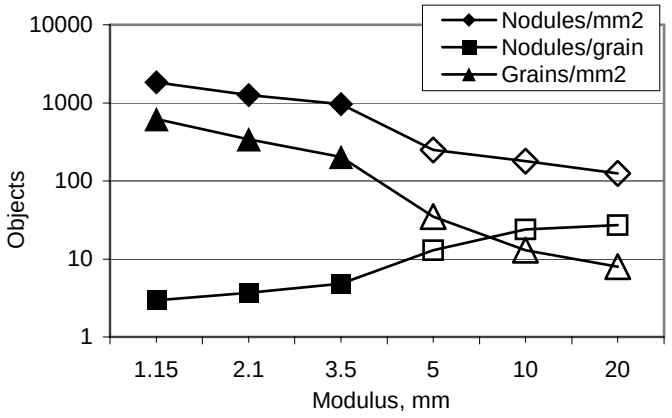

Fig. 6. Influence of casting modulus on the nodule count, grain count and number of nodules per grain. Present work data are shown with closed symbols and (Rivera, 1997) data with open symbols.

DISCUSSION

Based on previous work and on the experimental work discussed in this paper, the solidification sequence of eutectic SG iron may be summarized as shown in Fig. 7. It is reasonable to assume that, at the beginning of eutectic solidification, both graphite nodules and austenite crystals are nucleating independently in the liquid. Natural convection will move both phases and no significant interaction between graphite and austenite dendrites is expected, as shown in Fig. 7 (*a*). Once nucleated, the austenite dendrites will grow freely in the liquid. This is possible even though the composition is eutectic, as cast irons solidify following an asymmetric phase diagram. Because of convection, the small graphite spheroids will be swept by the growing austenite grains. While austenite dendrites grow, carbon is continuously rejected ahead of the interface, the viscosity of the solid-liquid mixture increases, and therefore the convection velocity decreases.

Based on limited measurements on directionally solidified SG iron samples, it is considered that the graphite-austenite interaction occurs when the fraction of solid reaches approximately 0.3, that is when dendrite coherency is established, because natural convection is suppressed Fig. 7 (*b*). This interaction is controlled by mechanisms similar to those controlling particle engulfment and pushing (PEP) (Stefanescu, 1999). A more detailed discussion of this interaction will be presented later in this paper. As a result of graphite particle-austenite dendrite interactions several nodules may be incorporated in one austenite grain.

The graphite particles grow isotropically by solid-state diffusion of carbon from the liquid through the austenite shell, to the graphite particle. The first graphite particles to be incorporated will have the longest time to grow and will be the largest nodules at the end of solidification. Smaller graphite spheroids will be found in the austenite closer to the interface, Fig. 7 (*c*).

To understand the interaction between austenite dendrites and graphite nodules in the early stages of solidification, the concepts developed for PEP may be used. As demonstrated for transparent organic materials (succinonitrile SCN - polystyrene particles system), a particle may be engulfed by the growing dendrite into the side of the dendrite arm, Fig. 8 (*a*), or through the splitting of the dendrite tip, Fig. 8 (*b*). Alternatively, the particle may be pushed in the interdendritic region, Fig. 8 (*c*), and entrapped in the last regions to solidify, process that will result in particle alignment.

A similar behavior may be inferred for the austenite-graphite eutectic system. This is schematically illustrated Fig. 7 (*b*). The contact between graphite and austenite dendrite can occur at the tip of the primary or secondary dendrite arms, position 1 in Fig. 7 (*b*) indicates a graphite particle after engulfment in the austenite dendrite.

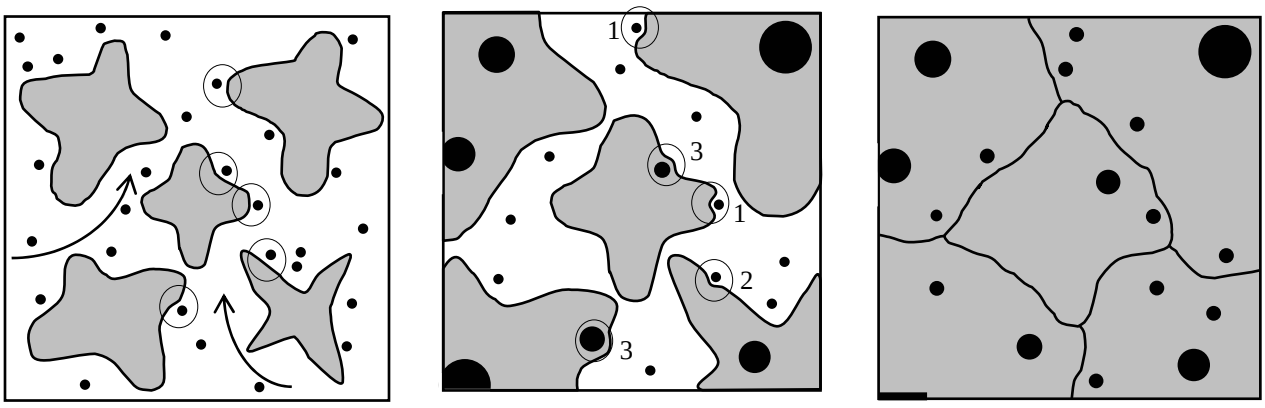

a) ***b)*** ***c)***

Fig. 7. Schematic drawing of the solidification sequences for a eutectic SG iron: (a) beginning of solidification, (b) graphite-austenite interaction during growth and (c) end of solidification.

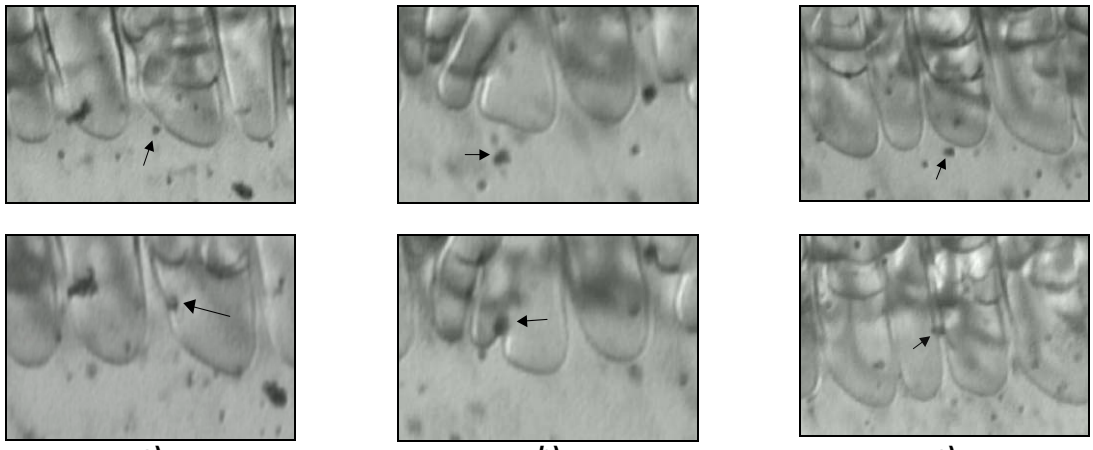

a) ***b)*** ***c)***

Fig. 8. Particle interface interaction during cellular/dendritic solidification of a SCN-polystyrene particles system (Stefanescu, in print): (a) engulfment into the side of the dendrite arm, (b) engulfment through dendrite tip splitting and (c) pushing and alignment between dendrite arms.

An example of graphite engulfment into the side of austenite dendrite is presented in Fig. 9 (*a*). Entrapment and alignment of SG is illustrated in Fig. 9 (*b*). The entrapped SG may be of normal size if the entrapment occurred early (Fig. 9 *b*), or of a very small size, approximately of 1 μm (Fig. 9 *c*), when graphite has grown only in the liquid and was entrapped in the last stage of solidification.

The engulfment of SG into the austenite dendrite can be explained as follows. In previous quenching experiments (Stefanescu, 1990) it was shown that the size of the graphite spheroids in this stage is about 1-1.5μm. Since the size of SG is very small, before the graphite-austenite interaction the austenite-liquid interface can be considered planar (Fig. 10 a). Once the convection level has decreased to the point where SG approaches the austenite-liquid interface, since graphite has higher thermal conductivity than austenite, a trough will grow at the graphite-austenite interface, which will allow the solid to grow around the particle (Fig. 10 b). The growth velocity of the solid is that of the austenite V_γ. As the solid rejects more carbon ahead of the interface, increasing the carbon content of the liquid, V_γ decreases. Carbon accumulation in the through, resulting from carbon rejection at the γ-L interface, will further contribute to the development of the through. Eventually, the SG particle will "dig" itself into the austenite (Fig. 10 c), and will be engulfed by it (Fig. 10 d). Up to this point, the graphite growth is very limited.

Once SG is engulfed, the eutectic grows with the velocity $V_{\gamma G}$ as a γ–graphite diffusion-couple in the regions where graphite was engulfed and with the velocity $V_\gamma$away from the diffusion couple (Fig. 10 *e*). During the diffusion-coupled growth the graphite acts as a sink for the carbon atoms rejected by the austenite, leaving less carbon to be rejected ahead of the solid-liquid interface. The overall result is a rapid advancement of the γ-*L* interface and a fast growth of the graphite inside the solid. The austenite growth is controlled by carbon diffusion, while the graphite growth is probably controlled by self-diffusion of Fe, as graphite needs space to expand into the surrounding solid. The diffusion-coupled growth of graphite and γ occur at higher velocities than the growth of the γ alone: $V_{\gamma G} > V_\gamma$ The presence of two different velocities at the solid-liquid interface will change the shape of the interface from concave (Fig. 10 *d*), to convex (Fig. 10 *e*).

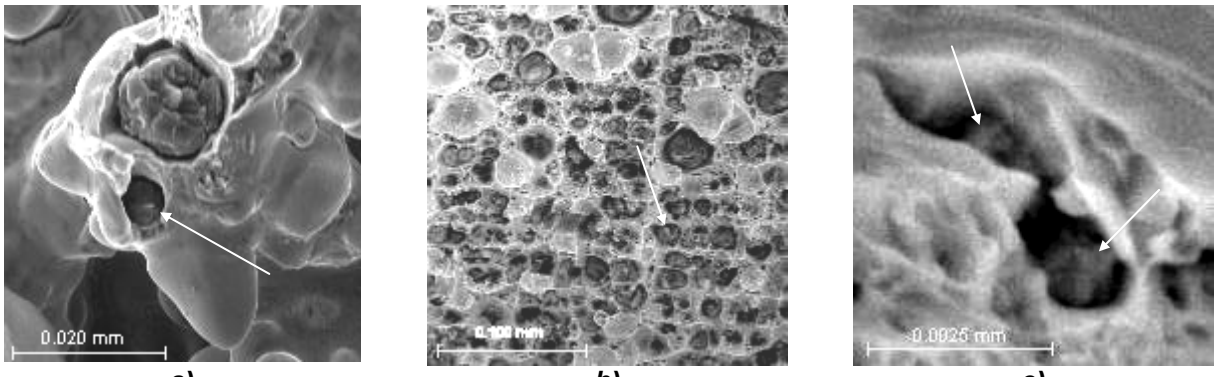

a) ***b)*** ***c)***

Fig. 9. Position of graphite particles and austenite at the interface in SG iron eutectic (SEM pictures): a) engulfed graphite particles, b) entrapped and aligned graphite particles and (c) small size entrapped graphite particles.

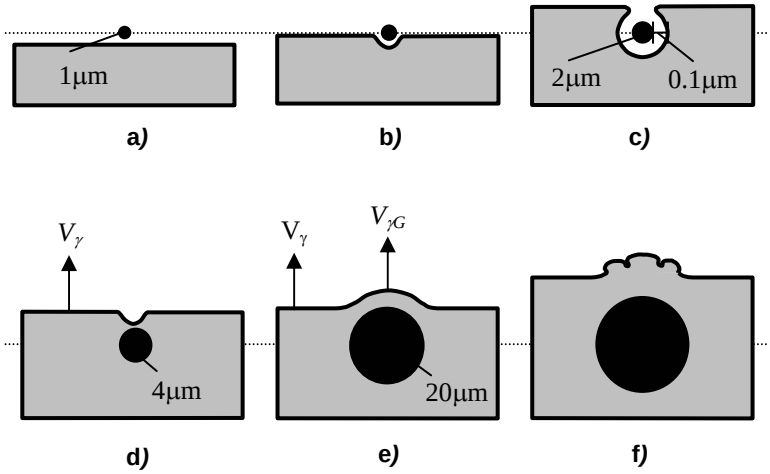

Fig. 10. Graphite-austenite interaction at the solid-liquid interface. The values for the graphite size and for the graphite-austenite gap are shown for discussion only. The drawings are not scaled to size.

The austenite growing into the liquid will tend to grow anisotropically in its preferred crystallographic orientation. However, restrictions imposed by the isotropic diffusion growth will impose an increased isotropy on the system. Consequently, the dendritic shape of the austenite will be altered and, as shown schematically in Fig. 10 *f*, the γ-*L* interface will exhibit only small protuberances instead of clear secondary arms. This is illustrated through the SEM pictures in Fig. 11. This process is dominant in the last regions to solidify.

This interpretation is consistent with recent phase-field modeling of dendritic growth. Karma et Rappel (Karma, 1998), have compared 3-dimensional growth of dendrites with cubic symmetry for the extreme cases of high anisotropy, Fig. 12 *a*, and no anisotropy, Fig. 12 *b*. It is seen that a metal with a cubic lattice will grow in a "cauliflower" shape in the absence of anisotropy. The SEM investigation showed remarkable similarities between the simulated and real austenite morphology for the case of isotropic growth (compare Fig. 12 *b* with Fig. 12 *c*).

According to the proposed mechanism, the final morphology of the eutectic grain will be as shown in Fig. 13, where a schematic representation of a eutectic γ-SG grain is compared to a eutectic SG grain as outlined by color metallography. The pattern respects all the important features that were discussed as supporting evidence for the proposed mechanism of the eutectic solidification of SG cast iron.

THEORETICAL WORK

MODEL DESCRIPTION

The proposed model uses the cellular automaton approach with deterministic rules to account for nucleation and growth in equiaxed dendritic and eutectic grains of an SG iron of exact eutectic composition. The model is applied over a cubic 3-dimensional simulation domain of 200 μm side that is divided in cells of 1 μm^3. The cells are identified by an index defining the solid or liquid state and the grain to which they belong. The domain is assumed isothermal. Constant heat extraction is imposed.

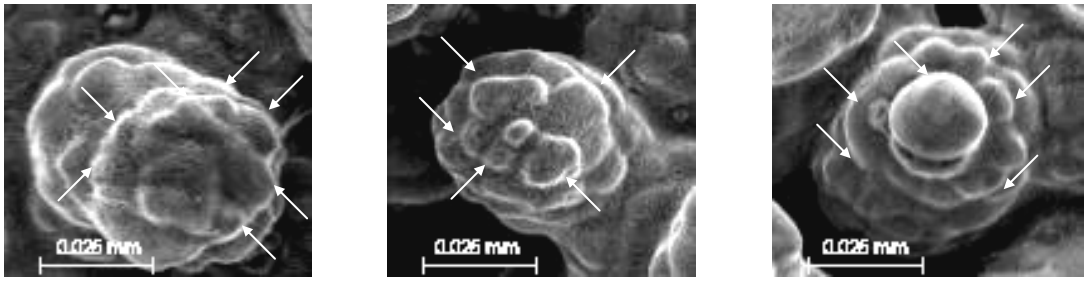

(a) ***(b)*** ***(c)***

Fig. 11. Typicall shape of the tip of the arms of SG eutectic dendrites (SEM pictures).

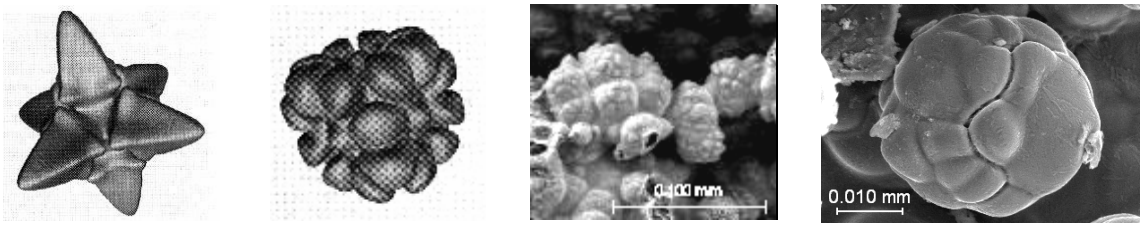

(a) **(b)** **(c)**

Fig. 12. Simulated growth of the dendrite morphology (Karma, 1998) and real dendrite morphology: (a) simulated growth with high anisotropy, (b) simulated growth without anisotropy and (c) SG eutectic dendrites where the loss of anisotropy lead to an effective modification of the dendrite morphology (SEM pictures).

After reaching the nucleation or transformation temperature, the cells in the domain are allowed to change the value of their indexes. This is done according to the deterministic rules described in the Nastac-Stefanescu model for equiaxed dendrite austenite grains (Nastac, 1996) and (Chang, 1992) for equiaxed eutectic grains. The fraction of solid is evaluated at all time steps from the ratio of solid cells to the total number of cells in the domain. The growth of the eutectic grains is triggered only after an austenite dendrite touches a graphite nucleus. The nucleus transforms into a graphite nodule developing an austenite shell that is considered an integral part of the original dendritic grain.

NUCLEATION

Nucleation is assumed to occur simultaneously and randomly in the domain for the primary austenite grains and the graphite nuclei. Instantaneous nucleation is assumed for both phases. The number of austenite grains is obtained from some standard correlation of grain density with cooling rate and undercooling as shown in Equation 1. To obtain the final density of grains this equation is integrated over the estimated solidification time, which for the present model was taken as 10 s. The undercooling was considered to be the maximum undercooling, which for this model was 10°C.

$$\frac{\partial N}{\partial t} = -n\mu_1 (\Delta T)^{n-1} \frac{\partial T}{\partial t} \qquad \text{Equation 1}$$

where N is the number of grains, T is temperature, t is time, μ_1 is the growth constant, and n is an exponent. The values used are (Tian, 1993): $n = 0.93$ and $\mu_1 = 2.45$.

There are no further restrictions regarding the austenite nucleus positions. The location of the austenite grain is indicated in the domain by assigning an integer value to the cell where it is placed. This integer represents a grain of 1 μm^3 initial size.

For the case of the graphite, it is assumed that the number of nuclei is higher than the final volumetric density of the graphite nodules. The density of initial graphite nuclei is around $2.5 \cdot 10^6$ mm^{-3}. The graphite nuclei are all represented by the same integer, assigned to their nucleation cells having also a size of 1 μm^3.

GROWTH OF AUSTENITE EQUIAXED GRAINS

After nucleation, the equiaxed austenite grains are the only ones allowed to grow. They grow as spheres according to the following equations (Tian, 1993):

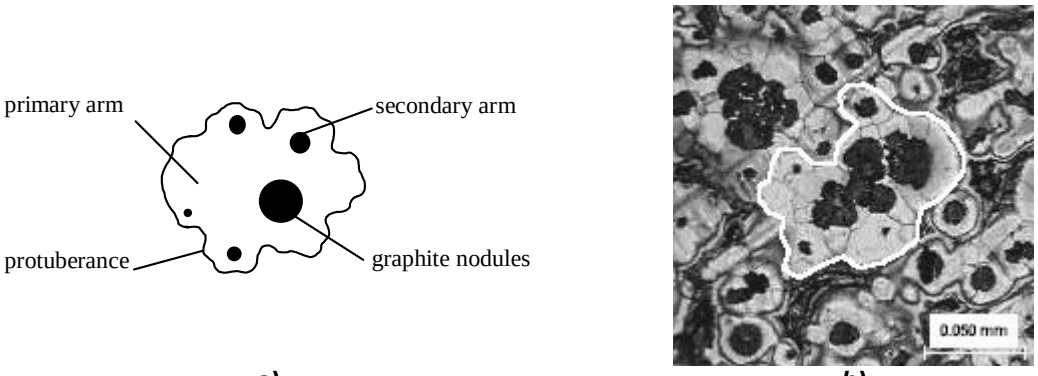

a) ***b)***

Fig. 13. Pattern of a γ-SG grain: a) cross-section representation of a γ-SG grain; b) eutectic γ-SG grain as outlined by color metallography.

$$V = \mu \Delta T^2 \qquad \text{Equation 2}$$

$$\mu = \frac{2\sigma^*}{\Gamma}\left[\frac{m(k-1)C_L^*}{D_L} + \frac{\rho L}{K_L}\right]^{-1} \qquad \text{Equation 3}$$

where V is the velocity of the spherical interface, μ is the growth factor, σ^* is a stability constant, m is the slope of the liquidus line, k is the partition coefficient, Γ is the Gibbs-Thompson coefficient, L is the latent heat of fusion, K_L is the thermal conductivity of the liquid, D_L is the liquid diffusivity. The liquid concentration, C_L^*, is calculated with the Nastac-Stefanescu model (Nastac, 1993).

GROWTH OF THE DIVORCED EUTECTIC IN DUCTILE IRON

The growth of the divorced eutectic in ductile iron is simulated assuming that once an austenite grain touches a graphite nucleus then the graphite starts growing through carbon diffusion through the austenite shell that envelops it. The austenite shell grows according to the following equation (Chang, 1992):

$$\frac{dR_\gamma}{dt} = D_C^\gamma \frac{R_G}{(R_G - R_\gamma)R_\gamma}\frac{C^{G/\gamma} - C^{L/\gamma}}{C^{\gamma/L} - C^{L/\gamma}} \qquad \text{Equation 4}$$

where the subscripts γ and G indicate the austenite and the graphite, respectively. After the formation of the austenite shell around the graphite nodule it is considered that the primary austenite, the austenite shell, and the graphite have become a eutectic grain. The growth of the graphite nodule can be calculated from mass balance according to the following equation (Chang, 1992):

$$\rho_G \frac{4}{3}\pi\left[\left(R_G^{t+\Delta t}\right)^3 - \left(R_G^t\right)^3\right] = \rho_\gamma \Delta V_\gamma C^{L/\gamma} \qquad \text{Equation 5}$$

The composition of the liquid at the interface $C^{\gamma/L}$ is calculated as C_L^*, and from it the austenite composition is calculated as $C^{L/\gamma} = kC^{\gamma/L}$. The remaining composition of the austenite at the interface with graphite $C^{G/\gamma}$ is calculated from the phase diagram.

The austenite in the primary phase and the shell are considered to form a single grain. In the present model it is possible for a single austenite grain to touch several graphite nuclei. This allows a eutectic grain to have multiple nodules. All of this leads to the following scenario in the present model:

- Austenite grains start growing at the liquidus temperature for a hypoeutectic iron or at the eutectic temperature for an iron of eutectic composition.
- Graphite nodules start growing (are activated) after making contact with austenite grains.
- The austenite shell around a nodule can in turn touch another graphite nucleus, transforming it into a nodule with its own austenite shell.
- The original austenite grain and all the nodules activated by this grain and subsequent shells form one eutectic grain.

The dendritic growth of the primary phase described by Equation 2 is significantly slower than the eutectic growth. The result is that the first austenite grain that touches a graphite nucleus will grow much faster than those that have not yet reached a graphite nucleus. Therefore, only a few austenite grains will become eutectic grains. Thus, if we assume that the density of initial graphite nuclei is the same as the nodule density obtained from experimental data, the microstructure predicted by the model will produce a significantly smaller amount of eutectic grains than those found experimentally.

The requirement of a higher initial density of graphite nuclei can be understood if it is accepted that, once activated, a graphite nodule depletes the surrounding volume of carbon and no further nodules can grow in this volume. This exclusion zone defines the separation distance between nodules in the same eutectic grain.

Table 3. Simulation Parameters

Simulation domain	200x200x200 μm
Number of austenite grains N	60
Number of graphite nuclei N_q	20000
Partition coefficient k	0.49
Diffusion in the liquid austenite D_L	$5 \cdot 10^{-9}$ m^2 s^{-1}
Diffusion in the solid austenite D_S	$1.5 \cdot 10^{-10}$ m^2 s^{-1}
Density of the austenite ρ_γ	7000 Kg m^{-3}
Density of carbon ρ_G	2220 Kg m^{-3}
Thermal conductivity of austenite K_γ	30 W m^{-1} K^{-1}
Specific heat of austenite Cp	880 J Kg^{-1} K^{-1}
Latent heat of fusion of metal H	$1.85 \cdot 10^5$ J Kg^{-1}
Stability constant σ^*	$(2\pi)^{-2}$
Gibbs-Thomson coefficient Γ	$2 \cdot 10^{-7}$ m K
Time step	0.1 s

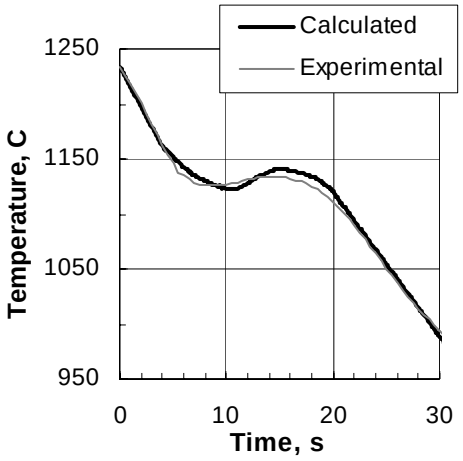

Fig. 14. Calculated and experimental cooling curves.

RESULTS

The new model was coupled with an existing model that simulated heat transfer for a plate (Chang, 1992). The purpose of this coupling was to match the experimental curve of a given plate. The cooling curve predicted by the model was matched to the experimental by adjusting the parameters of austenite grains and exclusion zone around a nodule. The best fit was achieved using 60 austenite grains assumed to nucleate in the domain of 200 μm by side. The exclusion distance (radius) around an activated nodule was 26 μm. The values of the simulation parameters are shown in Table 3.

The experimental and calculated cooling curves are shown in Fig. 14. The experimental curve was obtained from a 3 mm thick plate. For the calculated curve, note that the maximum undercooling below the eutectic temperature is determined by the size that an austenite grain can grow before touching a graphite nucleus. For a fixed density of graphite nuclei, this maximum undercooling depends on the nucleation rate of austenite grains. The exclusion distance around an activated graphite nucleus determines the recalescence. The smaller this distance is the higher and faster the incremental growth in temperature becomes right after the maximum undercooling.

The model is able to draw a realistic representation of the grain structure during the solidification process. This is shown in Fig. 15. The solidification sequence is shown at 0.25, 0.5, 0.75, and 0.99 solid fraction. This sequence is obtained by sectioning at the center the 3-D domain used in calculations.

Image analysis was performed on the computer output (drawings) of the calculated microstructure at 0.99 solid fraction. Ten sections at different levels of the same domain were analyzed. The technique used was similar to that described earlier for the analysis of colored etched samples. The results are compared in Table 4 to the experimental results obtained from Fig. 6 by interpolation for a thickness of 3 mm.

Table 4. Comparison of Experimental and Calculated Values of Microstructural Features

Microstructural features	Experimental	Calculated
Nodules/grain	3.2	1.4
Nodules/mm^2	1625	535
Grains/mm^2	515	434

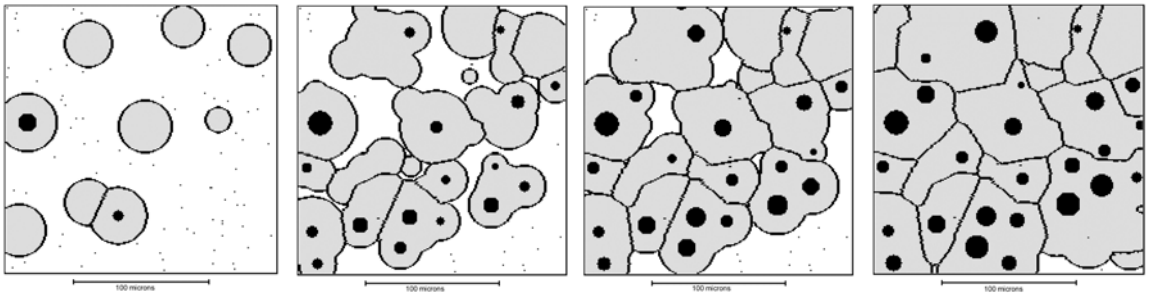

a) f_S = 0.24 ***b) f_S = 0.55*** ***c) f_S = 0.72*** ***d) f_S = 0.99***

Fig. 15. Model output of microstructure evolution of eutectic SG iron during solidification.

DISCUSSION

When analyzing the data presented in Table 4 it is noticed that the number of calculated eutectic grains is slightly smaller than the experimental number, but the calculated nodule count is significantly lower. Note that, as previously mentioned, the real number of eutectic grains is in fact smaller than that measured using color etching. The number of eutectic grains is similar in the experiments and the model because of the experimental correlation used to estimate their amount, and because the calculated cooling curve was matched to the experiment by adjusting the number of eutectic grains and exclusion zone around a nodule. The discrepancy between the calculated and measured nodule count is caused mostly by the concept of the exclusion zone. This exclusion zone defines the minimum nodule size that can be accounted for in the model.

CONCLUDING REMARKS

The *in-situ* solidification morphology of SG iron was investigated in the micro-shrinkage cavities of thin plates. Two types of austenite dendrites were observed: primary dendrites exhibiting the classical morphology of dendrites, and eutectic SG dendrites have a significantly different morphology. As the primary and the secondary arms have almost the same length, the distinction between the two is not so clear. The tips of the dendrite arms are thick and rounded to accommodate the spheroidal graphite particles. Small protuberances were observed on the surface. One of the most important features revealed during the SEM investigation was that the multi-nodular nature of these dendrites.

Using color etching metallography it was confirmed that each austenite grain contains several graphite nodules. The number of grains per square millimeter and the number of nodules by grain were quantified. It was found that the grain count decreases faster with the casting modulus than the nodule count. This finding may have significant implications when attempting to develop microstructure-mechanical properties models.

The experimental evidence presented in this paper showed that the interaction between graphite nodules and austenite is controlled by a similar mechanism to that controlling particle engulfment and pushing (PEP). At the beginning of the interaction between graphite nodules and austenite, a trough develops on the interface because graphite has higher thermal conductivity than the matrix. This trough will allow the austenite to grow around the graphite engulfing it. Then, the austenite-graphite grain will grow rapidly. Austenite growth is controlled by carbon diffusion, while the graphite growth is controlled by self-diffusion of Fe, as graphite needs space to expand into the surrounding solid. The eutectic will grow faster than the adjacent austenite. The growth product will be a eutectic dendrite containing spheroidal graphite.

A new 3-D model for solidification of eutectic SG iron was developed using a combined deterministic - stochastic approach. The model incorporates the features observed in the metallographic study, which are the presence of two types of dendrites, and the multi-nodular nature of the eutectic grain. At the end of the solidification, the two types of dendrites cannot be distinguished.

The calculated and experimental cooling curves agree reasonably well. The calculated microstructure resembles closely the delineation of grains obtained by the coloration etching technique. Although the nodule count calculated by the model was lower than the experimentally measured one, the model was able to reproduce the multi-nodular morphology of the eutectic grain.

ACKNOWLEDGMENTS

This research has been funded by a consortium of foundries and foundry suppliers and by the Metal Casting Competitiveness Program of the U. S. Department of Energy (DOE Cooperative Agreement DE-FC07-94ID13324). However, any opinions, findings, conclusions, or recommendations expressed herein are those of the authors and do not necessarily reflect the views of DOE. The authors acknowledge the active support of the industrial sponsors, without which the program could not have succeeded. Particular gratitude is extended to Dr. T. Piwonka, Director of the Metal Casting Technology Center at the University of Alabama for his continuous encouragement and his unselfish gift of time during many discussions on the subject.

REFERENCES

Boeri, R., Weinberg F., Microsegregstion in Ductile Iron, *AFS Transactions*, pp 179-184 (1989)

Chang, S., Shangguan, D., Stefanescu, D. M., *Metallurgical Transactions A*, vol. 23A, pp 1333-1346 (1992)

Charbon, C., Rappaz, M., *Advanced Materials Research*, No 4-5, p 453 (1997)

Fras, E., Kapturkiewicz, W., Burbielko A. A., *Modeling of Casting, Welding and Advanced Solidification Processes VII*, M. Cross and J. Campbell eds., The Minerals, Metals & Materials Society, pp 679-686 (1995)

Fras, E., Lopez, H. F., *Metallurgical and Materials Transactions B*, vol. 30B, pp 927-932 (1999)

Fredriksson, H., Svensson, I. I., A Comparison between the Growth Processes of Cast Iron by Thermal Analysis, *Proceedings of Solidification Processing of Eutectic Alloys*, The Metallurgical Society (1988)

Gandin, Ch. A., Jalanti, T., Rappaz, M., *Modeling of Casting, Welding and Advanced Solidification Processes VIII*, B.G. Thomas and C. Beckermann eds., The Minerals, Metals & Materials Society, pp 363-374 (1998)
Karma, A., Rappel, W-J, *Physical Revue E*, No. 4, vol. 57, pp 4323-4349 (1998)
Kobayashi, T., Kawabe, N., Imuca, T., *Jpn. J. Appl. Phys*., vol. 26 (11), pp 1823-1829 (1987)
Loper Jr., C. R., Heine, R. W., Graphite Formation during Solidification of Cast Iron, *AFS Transactions*, pp 583-600 (1962)
Lux, B., Mollard, F., Minkoff, I., *The Metallurgy of Cast Iron*, B. Lux, I. Minkoff, and F. Mollard eds., Georgi Publ. Comp., St. Saphorin, Switzerland, pp 371-403 (1974)
Motz, J M., Microsegregations-an Easily Unnoticed Influencing Variable in the Structure Description of Cast Materials, *Practical Metallography*, vol. 30, pp 122-128, (1988)
Nastac, L., Stefanescu, D.M., *Metallurgical and Materials Transactions A*, vol. 24A, pp 2107-2118 (1993)
Nastac, L., Stefanescu, D.M., *Metallurgical and Materials Transactions A*, vol. 27A, pp 4061-4074 (1996)
Patterson, W., Über den Einfluss von Fremdkeimen auf die Kristallisation von Metallen und Legierungen, insbesondere auf die Ausbilkdung des Eutectikums in Gusseisen, *Giesserei Techn*, Wissensch, Beihefte, pp 355-378, (1952)
Rickert, A., Engler, S., *The Physical Metallurgy of Cast Iron*, edited by H. Fredriksson and M. Hillert, Mater. Res. Soc. Proc. 34, Pittsburgh, PA, pp 165 (1985)
Rivera, G., Boeri, R., Sikora, J., Counting Eutectic Grains in SG Cast Iron, *Advanced Materials Research*, vol. 4-5, pp 169-174 (1997)
Schmidt, F. A., Mason, J. T., Trivedi, R, *Metallography*, No. 18, pp 35-40 (1985)
Stefanescu, D.M., *ASM Handbook*, 9th ed, vol. 15, Metals Park, OH, pp 168-181 (1992)
Stefanescu, D. M., Bandyopadhyay, D. K., On the Solidification Kinetics of Spheroidal Graphite Cast Iron, *Physical Metallurgy of Cast Iron*, G. Ohira, T. Kusakawa and E. Niyama eds., Materials Research Soc., Pittsburgh, PA, pp 15-26 (1990)
Stefanescu, D.M., Pang, H., *Canadian Metallurgical Quarterly*, vol. 37, No. 3-4, pp 229-239 (1998)
Stefanescu, D. M., *Cutting Edge of Computer Simulation and Casting*, I. Ohnaka editor, ISIJ Osaka, Japan, (1999)
Stefanescu, D. M., Catalina, A.V., Juretzko, F. R., Mukherjee, S., Sen, S., Dhindaw, B.K., Particle Engulfment and Pushing Micro-gravity Experiments and Mathematical Modeling, *First International Symposium on Microgravity Research and Applications in Physical Science and Biotechnology*, Sorento, Italy, in print (2000)
Tian, H., Stefanescu, D.M., Dendritic Growth during Directional Solidification of Hypoeutectic Fe-C-Si Alloys, *Metallurgical Transactions A*, vol. 23, pp 681-687 (1992)
Tian, H., Stefanescu, D.M., *Modeling of Casting, Welding and Advanced Solidification Processes VI*, T.S> Piwonka , V. Voller, and L. Katgerman eds., The Minerals, Metals & Materials Society, pp. 639-646 (1993)
Van de Velde, A., *AFS Special Report - The Solidification of Ductile Cast Iron – A New Approach*, Des Plaines, IL, (1997)
Wang, C.Y., Beckerman, C., *Metallurgical Transactions A*, vol. 27A, pp 2754-2795 (1996)